

# Non-collapsing electric readout of arbitrary Andreev qubits

Xian-Peng Zhang,<sup>1,2</sup> Chuanchang Zeng,<sup>1</sup> Zhen-Biao Yang,<sup>3</sup> Jose Carlos Egues,<sup>4,\*</sup> and Yugui Yao<sup>1,†</sup>

<sup>1</sup>Centre for Quantum Physics, Key Laboratory of Advanced Optoelectronic Quantum Architecture and Measurement (MOE), School of Physics, Beijing Institute of Technology, Beijing, 100081, China

<sup>2</sup>Department of Physics, Hong Kong University of Science and Technology, Clear Water Bay, Hong Kong, China

<sup>3</sup>Fujian Key Laboratory of Quantum Information and Quantum Optics, College of Physics and Information Engineering, Fuzhou University, Fuzhou, Fujian 350116, China

<sup>4</sup>Instituto de Física de São Carlos, Universidade de São Paulo, 13560-970 São Carlos, São Paulo, Brazil

Nondemolition protocols use ancilla qubits to identify the fragile quantum state of a qubit without destroying its encoded information, thus playing a crucial role in nondestructive quantum measurements particularly relevant for quantum error correction. However, the multitude of ancilla preparations, information transfers, and ancilla measurements in these protocols create an intrinsic overhead for information processing. Here we consider an Andreev qubit defined in a quantum-dot Josephson junction and show that the intrinsic time-dependent oscillatory supercurrent arising from the quantum interference of the many-body eigenstates of the Andreev qubit, can be used to probe the qubit itself nondestructively and *without* collapsing its quantum state. This nondestructive and non-collapsing readout of arbitrary superposition states of Andreev qubits avoids ancilla qubits altogether and significantly reduces experimental overhead as no repetitive qubit resetting is needed. Our findings should have an unprecedented impact on advancing research and applications involving Andreev dots, thus positioning them as promising qubit contenders for quantum processing and technologies.

## I. INTRODUCTION

Andreev qubits [1, 2], combining the extraordinary scalability of superconducting circuits and the compact footprint of quantum dots, offer tremendous potential for advancements in quantum science and technology [3–12]. An exciting subject is the coherent manipulation of Andreev qubits within hybrid quantum electrodynamics architectures [9–15]. In conventional quantum computation and information, the readout of a qubit state inherently collapses the qubit state into one of the artificially preselected basis states (e.g. the alive and dead Schrödinger’s cat states) and thus generally destroys the previously prepared quantum state and its encoded information [16]. The qubit-state collapse during readout follows from the thought-to-be fundamental tenet of measurements in quantum mechanics, establishing the foundations for the no-cloning theorem [17].

To identify quantum states without destroying the encoded information, quantum nondemolition measurements have been developed [18–36]. These protocols rely on transferring and temporally storing the encoded qubit information to a well-prepared ancilla, which is then measured. Although the repetitive measurements of the ancillae can be destructive, the original qubit state remains intact and retrievable. The ancilla-based repetitive quantum nondemolition readout has been a common approach across various platforms, such as trapped ions [23, 24], superconducting spin qubits [14], quantum-dot spin qubits [20, 22], cavity quantum electrodynam-

ics systems [25–28], electron-nuclear spin qubits [29–32], and superconducting qubits [34–36]. Even though these techniques have demonstrated significant progress, they introduce large-scale ancilla preparations, information transfers, and ancilla measurements [24], which are still expensive, laborious, and time-consuming in realistic experiments.

In this work, we show that Andreev qubits formed in a quantum-dot Josephson junction [Fig. 1(a)] can be used to overcome the shortcomings and overhead of nondemolition measurement protocols. Our proposal benefits from an Andreev qubit carrying an intrinsic macroscopic supercurrent that is a unique fingerprint of its encoded quantum information. Remarkably, we explicitly show how an ordinary supercurrent measurement can probe an Andreev qubit – nondestructively and *without* collapsing its quantum state. More specifically, by time evolving the system exactly, we find that the supercurrent of an arbitrary superposition state  $|X\rangle = \cos(\theta/2)|0\rangle + \sin(\theta/2)e^{i\vartheta}|1\rangle$  [see the two angles  $\theta$  and  $\vartheta$  in Fig. 1(b)] has both static [Eq. (3)] and dynamic [Eq. (4)] contributions. The static part, calculated from the time average of the total supercurrent, determines the azimuthal angle  $\theta$ , while the dynamic part, originating from the quantum interference between many-body eigenstates and exhibiting an oscillatory pattern analogous to the usual alternating-current Josephson effect, specifies the polar angle  $\vartheta$  [Fig. 1(c) and Fig. 3(a)]. We simulate the detrimental effects of experimental non-idealities in the current measurements and verify that our readout protocol has fidelities within the threshold for quantum error correction [Fig. 3(b)]. Our nondestructive Andreev qubit readout eliminates the qubit state collapse – a crucial feature of quantum measurement – and

\* egues@ifsc.usp.br

† ygyao@bit.edu.cn

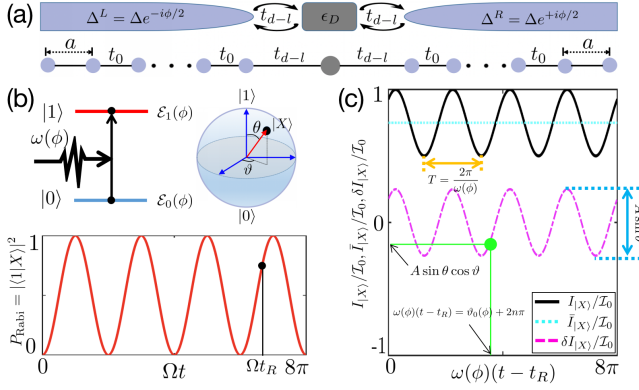


Figure 1. (a) Sketch of a quantum-dot Josephson junction. A quantum dot (gray), gate-defined in an InAs nanowire (red), is tunnel coupled to proximitized InAs/Al left (L) and right (R) superconducting leads (blue) with phase bias  $\phi = \phi_R - \phi_L$ . The lower panel denotes the corresponding 1D tight-binding model. (b) Preparation of an arbitrary Andreev quantum-dot qubit state: upon resonant microwave driving [ $\hbar\omega(\phi) = \mathcal{E}_1(\phi) - \mathcal{E}_0(\phi)$ ], the qubit undergoes Rabi oscillations between states  $|0\rangle$  and  $|1\rangle$  with Rabi frequency  $|\Omega|$  [lower panel in (b)]. Arbitrary qubit states  $|X\rangle = \cos(\theta/2)|0\rangle + \sin(\theta/2)e^{i\vartheta}|1\rangle$  can be prepared on the Bloch sphere, where the azimuthal angle  $\theta \in [0, \pi]$  is adjusted by the microwave pulse duration  $t_R$  and the pole angle  $\vartheta \in [0, 2\pi]$  is controlled by the angle of the Rabi amplitude  $\Omega$ , i.e.,  $\vartheta = \text{angle}(\Omega)$ . For instance, the black dot on the Rabi oscillation curve corresponds to  $(\theta, \vartheta) = (\pi/6, \pi/3)$ . (c) Non-collapsing readout of Andreev qubits from the time evolution of the phase-biased supercurrent  $I_{|X\rangle} = I_{|X\rangle}^S + A(\phi) \sin \theta \cos[\omega(\phi)(t - t_R) - \varphi_0(\phi) - \vartheta]$  corresponding to the arbitrary superposition  $|X\rangle$  in (b), where  $A(\phi) = 2e\omega(\phi)|\mathcal{C}_{0,1}(\phi)|$ , with  $\mathcal{C}_{0,1}(\phi) = \langle 0|\partial_\phi|1\rangle = |\mathcal{C}_{0,1}(\phi)|e^{i\varphi_0(\phi)}$ . For a given experimental run, the phase bias  $\phi$  and the gate-tunable dot level  $\epsilon_D$  are kept fixed and so are  $\omega(\phi)$ ,  $\varphi_0(\phi)$ ,  $|\mathcal{C}_{0,1}(\phi)|$ ,  $I_{|0\rangle}$  and  $I_{|1\rangle}$ . The static supercurrent  $I_{|X\rangle}^S = \cos^2(\theta/2)I_{|0\rangle} + \sin^2(\theta/2)I_{|1\rangle}$ , calculated from the time average of the total supercurrent, determines  $\theta$ , which also controls the oscillation amplitude of the interference supercurrent, i.e.,  $A(\phi) \sin \theta$ . The qubit parameters,  $\omega(\phi)$  and  $\vartheta$ , can be read out from the oscillation period  $2\pi/\omega(\phi)$  and the interference supercurrent  $A(\phi) \sin \theta \cos \vartheta$  at  $\omega(\phi)(t - t_R) = \varphi_0(\phi) + 2n\pi$ , respectively. Other parameters are the same as Fig. 3.

obviates the extensive ancilla overhead (preparation, information transfer, measurements, etc), thus surpassing state-of-the-art quantum nondemolition measurements.

## II. MODEL SYSTEM

We consider a typical quantum-dot Josephson junction [12, 37, 38], depicted in Fig. 1(a), i. e., a quantum dot gate-defined in an InAs nanowire with dot energy  $\epsilon_D$ , tunnel-coupled to left ( $j = L$ ) and right ( $j = R$ ) proximitized InAs/Al leads with strength  $t_{d-l}$ . The leads have proximity-induced order parameters  $\Delta e^{i\phi_j}$  with a

flux-tunable phase difference  $\phi = \phi_R - \phi_L$ . Following the approach in Ref. [39], we describe this hybrid system by an effective continuum model which maps onto the above tight-binding model with identical left and right leads having chemical potentials  $\mu_S$  and nearest-neighbor tunneling amplitude  $t_0$  and discretization step  $a$  [lower panel of Fig. 1(a)]. This allows us to exactly diagonalize  $H = \sum_{l=1}^N \sum_{s=\uparrow/\downarrow} E_{ls}(\phi) \gamma_{ls}^\dagger(\phi) \gamma_{ls}(\phi) + \mathcal{E}_G$ , where  $N$  represents the system size, and  $s = \uparrow / \downarrow$  denotes the spin-up and -down Bogoliubons. The ground-state energy  $\mathcal{E}_G(\phi) = \mathcal{E} - \sum_{ls} \frac{1}{2} E_{ls}(\phi)$  is  $\phi$ -dependent, where the constant  $\mathcal{E}$ , irrelevant to our main result, is  $\phi$ -independent. The flux-tunable Bogoliubon operators associated with energy  $E_{ls}(\phi)$  are represented as unit vectors in the Nambu space:

$$\gamma_{ls}(\phi) = \sum_{n=1}^N [(u_s)_{ln} c_{ns} + (v_s)_{ln} (-s c_{n-s}^\dagger)]. \quad (1)$$

The field operator  $c_{ns}$  annihilates an electron with spin  $s$  at site  $n$ . The  $N \times N$  matrices  $u_s$  and  $v_s$  describe the electron and hole components of all Bogoliubons, respectively, which are  $\phi$ -dependent.

Quantum information processing based on Andreev qubits generally relies on the rigorous time evolution of the quantum-dot Josephson junction and thus demands precise many-body eigenfunctions, such as the ground-state eigenfunction. The flux-tunable many-body ground state, defined by  $\gamma_{ls}(\phi)|G\rangle = 0$  for all  $l$  and  $s$ , is full of Bogoliubov-like singlets

$$|G\rangle = \prod_{j=1}^N \frac{1}{N_j^{1/2}(\phi)} \left[ 1 + \mathcal{A}_{jj}(\phi) a_{j\uparrow}^\dagger(\phi) a_{j\downarrow}^\dagger(\phi) \right] |0\rangle_e, \quad (2)$$

where  $N_j(\phi) = 1 + |\mathcal{A}_{jj}(\phi)|^2$  and  $|0\rangle_e$  is the electron vacuum. The superconducting pairs  $a_{j\uparrow}^\dagger(\phi) a_{j\downarrow}^\dagger(\phi)$  show how the electrons in a non-uniform superconductor pair with each other (see expressions for  $\mathcal{A}_{jj}(\phi)$  and  $a_{js}^\dagger(\phi)$  in Ref. [40]). Interestingly, the flux-tunable superconducting pairs themselves carry an electrical signal of the macroscopic supercurrent - an inherent property of the superconducting state itself.

## III. INTERFERENCE SUPERCURRENT

Below we present the exact time evolution of the system and analytically derive the macroscopic supercurrent of an initial arbitrary superposition state. Hereafter, we only focus on the Andreev space, i.e., the low-energy sub-gap space of the quantum-dot Josephson junction. This is a good approximation when the in-gap Andreev levels  $[E_{ls}(\phi)$  with  $l = 1]$  are far away from the continuum spectra  $[E_{ls}(\phi)$  with  $l > 1]$ .

Let us consider the Andreev level qubit as an example. Its even-parity logic states are represented by the two flux-tunable low-energy many-body eigenstates  $|0\rangle = |G\rangle$

and  $|1\rangle = \gamma_{1\uparrow}^\dagger(\phi)\gamma_{1\downarrow}^\dagger(\phi)|G\rangle$  [1, 3, 7, 9], having energies  $\mathcal{E}_0(\phi) = \mathcal{E}_G(\phi)$  and  $\mathcal{E}_1(\phi) = \mathcal{E}_G(\phi) + E_{1\uparrow}(\phi) + E_{1\downarrow}(\phi)$ , respectively. In a hybrid quantum electrodynamics architecture [3, 9], the Andreev qubit coupling to microwave cavity photons allows one to prepare an arbitrary superposition  $|X\rangle$  of the logic states, i.e.,  $|X\rangle = \cos(\theta/2)|0\rangle + \sin(\theta/2)e^{i\vartheta}|1\rangle$  with  $\theta \in [0, \pi]$  and  $\vartheta \in [0, 2\pi]$ . These state vectors correspond to points  $(\theta, \vartheta)$  on a unity-radius Bloch sphere, Fig. 1(b).

We define the Josephson current of the arbitrary superposition state  $|X\rangle$  as the rate of change of the expectation value of electron number operators in the left or right lead:  $I_{|X\rangle} = +e\partial_t\langle X|N_L(t)|X\rangle = -e\partial_t\langle X|N_R(t)|X\rangle$  [41, 42] with  $N_j(t) = \sum_{n_s} c_{jns}^\dagger(t)c_{jns}(t)$ ; here the electron operators are in the Heisenberg picture, i.e.,  $c_{jns}(t) = e^{+iHt/\hbar}c_{jns}e^{-iHt/\hbar}$ . This microscopic definition describes the Josephson current as the intrinsic supercurrent that flows out of the left lead into the right lead with no applied voltage.

The supercurrent  $I_{|X\rangle}$  consists of two trivial terms  $e\cos^2(\theta/2)\partial_t\langle 0|N_j(t)|0\rangle$  and  $e\sin^2(\theta/2)\partial_t\langle 1|N_j(t)|1\rangle$  responsible for the static supercurrent  $I_{|X\rangle}^S$ , as well as two interference terms  $(e/2)\sin\theta e^{+i\vartheta}\partial_t\langle 0|N_j(t)|1\rangle$  and  $(e/2)\sin\theta e^{-i\vartheta}\partial_t\langle 1|N_j(t)|0\rangle$  contributing to the dynamic supercurrent  $I_{|X\rangle}^D$ , i.e.,  $I_{|X\rangle} = I_{|X\rangle}^S + I_{|X\rangle}^D$ . In passing, we note that when  $|X\rangle$  is a pure state corresponding to one of the qubit eigenstates, i.e.,  $|X\rangle = |m\rangle$ , with  $H|m\rangle = \mathcal{E}_m(\phi)|m\rangle$  for  $m = 0, 1$ , the dynamic contribution vanishes, i.e.,  $\delta I_{|X\rangle} = 0$ . In this case,  $I_{|X\rangle} = I_{|X\rangle}^S$  is entirely static and solely expressed as the  $\phi$  derivative of the corresponding eigenenergy, i.e.,  $I_{|m\rangle} = \mathcal{I}_0 \frac{\partial}{\partial \phi} \mathcal{E}_m(\phi)$ , where  $\mathcal{I}_0 = 2e/\hbar$  (see derivation in the Supplementary Materials (SM) [43]).

For the arbitrary superposition  $|X\rangle$  parametrized by  $(\theta, \vartheta)$  in Fig. 1(b), the static contribution  $I_{|X\rangle}^S$  can be expressed as a weighed sum of the static contributions from the eigenstates in the superposition, i.e.,

$$I_{|X\rangle}^S = \cos^2(\theta/2)I_{|0\rangle} + \sin^2(\theta/2)I_{|1\rangle}, \quad (3)$$

while the dynamic part  $I_{|X\rangle}^D$ , due to the interference between the qubit eigenstates, reads (see SM [43])

$$I_{|X\rangle}^D/\mathcal{I}_0 = \frac{1}{2}\sin\theta e^{-i\vartheta+i\omega(\phi)(t-t_R)}\hbar\omega(\phi)\mathcal{C}_{0,1}^*(\phi) + c.c., \quad (4)$$

where  $\omega(\phi) = [\mathcal{E}_1(\phi) - \mathcal{E}_0(\phi)]/\hbar$  and  $\mathcal{C}_{0,1}(\phi)$  is defined by the matrix element  $\mathcal{C}_{m,m'}(\phi) = \langle m|\partial_\phi|m'\rangle$ . Destructive interference occurs at degeneracy point for which  $\omega(\phi) = 0$ , resulting in a vanishing dynamical supercurrent. More importantly, the interference supercurrent in Eq. (4) can no longer be expressed in terms of the  $\phi$  derivatives of the eigenenergies as the supercurrent for pure states previously discussed. In contrast, the interference supercurrent here depends crucially on the  $\phi$  derivatives of the many-body eigenstates via the matrix

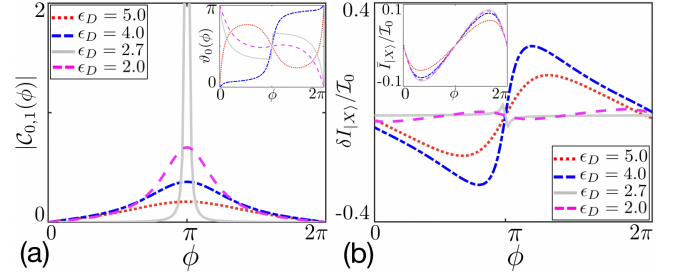


Figure 2. (a) Interference supercurrent  $I_{|X\rangle}^D = A\sin\theta\cos[\omega(\phi)(t-t_R) - \varphi_0(\phi) - \vartheta]$  as a function of  $\phi$  for different values of  $\epsilon_D$ . We consider the semiconducting quantum-dot Josephson junction, requiring sizable positive  $\epsilon_D$  (see SI [43]). This  $\phi$ -dependence stems from the qubit frequency  $\omega(\phi) = [\mathcal{E}_1(\phi) - \mathcal{E}_0(\phi)]/\hbar$  and the matrix element  $\mathcal{C}_{0,1}(\phi)$  in  $A = 2e\omega(\phi)|\mathcal{C}_{0,1}(\phi)|$ . We find a sizable interference supercurrent  $I_{|X\rangle}^D/\mathcal{I}_0 \simeq 0.2$ , which is even larger than the static supercurrent  $\bar{I}_{|X\rangle}$  plotted in the inset of panel (a). The small  $I_{|X\rangle}^D$  at  $\phi = \pi$  is due to  $I_{|X\rangle}^D$  being proportional to  $\omega(\phi)$  and  $\omega(\phi) \rightarrow 0$  as  $\phi \rightarrow \pi$ . (b) Absolute value of the matrix element  $\mathcal{C}_{0,1}(\phi) = \langle 0|\partial_\phi|1\rangle = \langle G|[\partial_\phi\gamma_{1\uparrow}^\dagger(\phi)]\gamma_{1\downarrow}^\dagger(\phi)|G\rangle$  as a function of the phase bias angle  $\phi$ , relying on the  $\gamma_{1\downarrow}(\phi)$  component of  $\partial_\phi\gamma_{1\uparrow}^\dagger(\phi)$ . The modulation of  $\gamma_{1\uparrow}^\dagger(\phi)$  with  $\phi$ , quantified by  $\partial_\phi\gamma_{1\uparrow}^\dagger(\phi)$ , is maximal around  $\phi = \pi$ , resulting in a large modulus of  $\mathcal{C}_{0,1}(\phi) = |\mathcal{C}_{0,1}(\phi)|e^{i\varphi_0(\phi)}$ ; the  $\varphi_0(\phi)$  is shown in the inset (b). Other parameters:  $\Delta = 1$ ,  $\theta = \pi/2$ ,  $\vartheta = 0$ ,  $t = t_R$ , and  $N = 903$ .

elements  $\mathcal{C}_{m,m'}(\phi)$ . It is convenient for our readout protocol to recast Eq. (4) as

$$I_{|X\rangle}^D/\mathcal{I}_0 = A(\phi)\sin\theta\cos[\omega(\phi)(t-t_R) - \varphi_0(\phi) - \vartheta], \quad (5)$$

This unique and sizable interference supercurrent fundamentally distinguishes an Andreev qubit from other qubits and highlights its quantum nature manifest macroscopically. Note that  $I_{|X\rangle}^D$  and  $I_{|X\rangle}^S$  are of the same order of magnitude.

Because  $|X\rangle$  is a superposition of eigenstates, it evolves in time according to  $|X(t)\rangle = \cos(\theta/2)e^{-i\mathcal{E}_0(\phi)(t-t_R)/\hbar}|0\rangle + \sin(\theta/2)e^{i\vartheta-i\mathcal{E}_1(\phi)(t-t_R)/\hbar}|1\rangle$  and the interference supercurrent ( $I_{|X\rangle}^D$ ) oscillates with time, Fig. 1(c), flowing back and forth persistently. This oscillatory behavior should be theoretically distinguishable from the alternating current Josephson effect arising from an applied voltage that induces a time-dependent flux  $\phi$ . Differently from the previous formulas in Refs. [44–46], the total supercurrent  $I_{|X\rangle} = I_{|X\rangle}^S + I_{|X\rangle}^D$  presented here contains not only the static supercurrent  $I_{|X\rangle}^S$ , quantified by the  $\phi$  derivative of the relevant eigenenergies [Eq. (3)], but also the unique dynamic supercurrent  $I_{|X\rangle}^D$  due to the interference between different many-body eigenstates [Eq. (4)].

To further analyze the interference supercurrent, we explore our theory numerically. The key to the interference supercurrent is the matrix elements  $\mathcal{C}_{r,r'}(\phi)$ .

Note that  $\langle G|\gamma_{1\uparrow}^\dagger(\phi)|x\rangle = 0$  for an arbitrary state  $|x\rangle$ , and hence we obtain  $\mathcal{C}_{0,1}(\phi) = \langle G|[\partial_\phi\gamma_{1\uparrow}^\dagger(\phi)]\gamma_{1\downarrow}^\dagger(\phi)|G\rangle$ . This means that only the  $\gamma_{1\downarrow}(\phi)$  component of  $\partial_\phi\gamma_{1\uparrow}^\dagger(\phi)$  contributes to the matrix element  $\mathcal{C}_{0,1}(\phi)$ , resulting in  $\mathcal{C}_{0,1}(\phi) = \sum_{n=1}^N [(v_\downarrow^*)_{1n}\partial_\phi(u_\uparrow^*)_{1n} - (u_\downarrow^*)_{1n}\partial_\phi(v_\uparrow^*)_{1n}]$ , where we have used the transformation (1). The interference supercurrent (4) reduces to  $I_{|X\rangle}^D = A(\phi) \sin\theta \cos[\omega(\phi)(t - t_R) - \varphi_0(\phi) - \vartheta]$  with  $A(\phi) = 2e\omega(\phi)|\mathcal{C}_{0,1}(\phi)|$  and  $\mathcal{C}_{0,1}(\phi) = |\mathcal{C}_{0,1}(\phi)|e^{i\varphi_0(\phi)}$ , where  $\varphi_0(\phi)$  denotes its phase.

Figure 2(a) shows the gate- and phase-tunable interference supercurrent  $I_{|X\rangle}^D$ . We obtain sizable dynamic supercurrents  $I_{|X\rangle}^D/\mathcal{I}_0 \simeq 0.23$ , even larger than the static contribution  $I_{|X\rangle}^S/\mathcal{I}_0$  plotted in the inset of Fig. 2(a). Thus, it is possible to reverse the sign of the supercurrent even the net supercurrent is fixed by the static supercurrent [see Fig. 3(a)]. This large interference supercurrent is due to the strong modulation of the eigenstates with respect to the phase  $\phi$ , as shown in Fig. 2(b), resulting in a large modulus of  $\mathcal{C}_{0,1}(\phi)$ , whose phase  $\varphi_0(\phi)$  is shown in the inset of Fig. 2(b). This sizable interference supercurrent is fundamentally important for Andreev qubits as it enables a direct detection of the qubit state without collapsing it as we discuss next.

#### IV. NON-COLLAPSING READOUT

One of the most remarkable applications of the interference supercurrent is the non-collapsing readout of an Andreev qubit. For a given setup with fixed  $\phi$  and  $\epsilon_D$ , the gate- and phase-dependent parameters such as  $\omega(\phi)$ ,  $\varphi_0(\phi)$ ,  $|\mathcal{C}_{0,1}(\phi)|$ ,  $I_{|0\rangle}$  and  $I_{|1\rangle}$  are also fixed and are detected before our readout procedures. The encoded information directly turns into an electrically measurable signal of the macroscopic supercurrent that, as shown in Fig. 1(c), oscillates with the frequency of the Andreev level qubit, i.e.,  $I_{|X\rangle} = I_{|X\rangle}^S + A(\phi) \sin\theta \cos[\omega(\phi)(t - t_R) - \varphi_0(\phi) - \vartheta]$  for  $t \geq t_R$ , where  $t_R$  is the microwave pulse duration for preparing the initial arbitrary superposition state [Fig. 1(b)]. The static supercurrent  $I_{|X\rangle}^S = \cos^2(\theta/2)I_{|0\rangle} + \sin^2(\theta/2)I_{|1\rangle}$  determines  $\theta$ , which is also present in the oscillation amplitude  $A(\phi) \sin\theta$ . The phase of the qubit state  $\vartheta$  can be extracted from the interference supercurrent at  $\omega(\phi)(t - t_R) = \varphi_0(\phi) + 2n\pi$  [or  $\omega(\phi)(t - t_R) = \varphi_0(\phi) + (4n + 1)\pi/2$ ], i.e.,  $I_{|X\rangle}^D = A(\phi) \sin\theta \cos\vartheta$  [or  $I_{|X\rangle}^D = A(\phi) \sin\theta \sin\vartheta$ ]. Moreover, setting  $\omega(\phi)(t - t_R) = 2n\pi$  allows for the recovery of the original qubit state, enabling the continuation of further processing. Figure 3 (a) shows the time oscillation of the total supercurrent for different values of  $(\theta, \vartheta)$ . The variation of  $\vartheta$  from 0 to  $\pi$  results in a  $\pi$  shift of the time oscillation. Additionally, the change of  $\theta$  from  $0.5\pi$  to  $0.2\pi$  has two effects on the supercurrent. First, it reduces the amplitude of the time oscillation. Second, it alters the static supercurrent from  $I_{|X\rangle}^S/\mathcal{I}_0 \simeq 0.028$  to

$I_{|X\rangle}^S/\mathcal{I}_0 \simeq -0.068$ . These findings demonstrate that both  $\vartheta$  and  $\theta$  play essential roles in determining the behavior of the macroscopic supercurrent.

The readout protocol proposed here surpasses previous approaches that require not only ancilla qubits but also repetitive resettings of the same initially prepared qubit state for its detection in subsequent times. That is, each subsequent detection point in the time evolution has to be obtained in a different run with the same reset initial state. The striking advantage of our proposed readout protocol is that it enables consecutive real-time measurements of the supercurrent without the overhead of the repetitive resetting. That is, using our protocol, for each run with a distinct *singly* prepared initial qubit state on the Bloch sphere, we can obtain *all* subsequent readouts in the time window of interest. This follows from our readout relying on only the measurement of the oscillatory supercurrent inherent to the initial qubit superposition state itself. Our readout obviates the collapse of the qubit state into one of its superposition basis states. As mentioned earlier, it remarkably affords a continuous (in time) non-collapsing and fully nondestructive measurement of the Andreev qubit state, thus retrieving its encoded information.

#### V. REAL-TIME DETECTION AND ERROR ANALYSIS

We now analyze the feasibility of our proposed non-destructive and non-collapsing readout. Recent experiments on the proximitized heterostructures have reported appreciable proximity-induced superconducting order parameters  $\Delta \sim 0.1$  meV [38]. The frequency of the macroscopic supercurrent  $\omega(\phi) \sim \Delta/\hbar$  can reach  $\sim 100$  GHz. This value corresponds to an oscillation period  $\sim 0.1$  ns, which is much longer than the time resolution of high-performance current meters  $\sim 1$  ps [47–50] and is much shorter than the coherence times of Andreev qubits  $\sim 100$  ns [9, 11].

We can extract the qubit state from the full time evolution of the total supercurrent [Figs. 1(c) and 3(a)]. During the experiments, however, it is inevitable that errors are introduced. We account for these effects by considering normally distributed variables with standard deviations in time  $\sigma_t$  and supercurrent  $\sigma_I$ . That is, we simulate the real-time supercurrent of each run according to  $I_{|X\rangle}(t_n) = \text{normrnd}[I_{|X\rangle}(t_n^c), \sigma_I]$ , with  $t_n^c = \text{normrnd}[t_n, \sigma_t]$  and  $t_n = n\delta t + t_R$ , where we set the time duration of detection to be  $\delta t = \pi/[10\omega(\phi)] \sim 0.01$  ns and  $\text{normrnd}[\mu, \sigma]$  generates a random number from the normal distribution with mean value  $\mu$  and standard deviation  $\sigma$ .

To quantify the readout efficiency of each run with the experimental errors ( $\sigma_{t,I} \neq 0$ ), we define an infidelity as  $\mathcal{F}(X, X') = 1 - |\langle X|X'\rangle|^2$ , where  $|X'\rangle$  is the measured state for each singly prepared distinct initial  $|X\rangle$  and is read from the time-dependent supercurrent  $I_{|X\rangle}(t_n)$

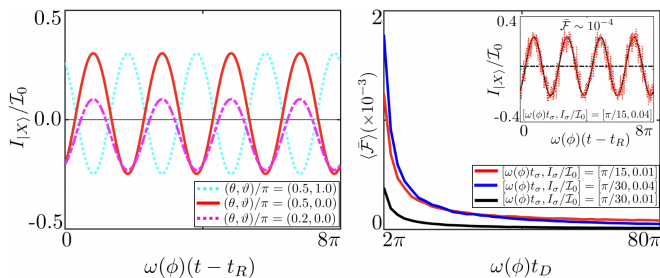


Figure 3. (a) Ideal non-collapsing supercurrent readout for different initial qubit states  $|X\rangle$  parametrized by  $(\theta, \vartheta)$  in the Bloch sphere [Fig. 1(b)]. The oscillatory supercurrent obeys  $I_{|X\rangle} = I_{|X\rangle}^S + A(\phi) \sin \theta \cos[\omega(\phi)(t - t_R) - \varphi_0(\phi) - \vartheta]$ . The angles  $(\theta, \vartheta)$  can be chosen by resonantly Rabi driving the Andreev qubit. By varying  $\vartheta$  from 0 (red) to  $\pi$  (cyan), we see a  $\pi$  shift of the supercurrent oscillation. Changing  $\theta$  from  $0.5\pi$  (red) to  $0.2\pi$  (magenta) not only reduces the amplitude of the oscillations but also modifies the static supercurrent (3) from  $I_{|X\rangle}^S/I_0 \simeq 0.028$  to  $I_{|X\rangle}^S/I_0 \simeq -0.068$ . (b) The infidelity  $\langle \bar{\mathcal{F}}(\sigma_t, \sigma_I) \rangle$  – averaged over both the full Bloch sphere and a large number of runs simulating experimental current and time uncertainties in the measurements – substantially decreases with increasing total detection time  $t_D$ , where  $|X'\rangle$  denotes the imperfect measured state corresponding to a given  $|X\rangle$  arising from the simulated uncertainty in the measured current and time evolution. Though a significant standard deviations in time and supercurrent results in a relatively poor signal as seen in the inset of Fig. 3(b), which shows three runs (i.e., green, blue, and magenta curves) of real-time supercurrent chosen randomly, we still attain small infidelity  $\bar{\mathcal{F}}(X, \sigma_t, \sigma_I) \sim 10^{-3}$  for fixed  $(\theta, \vartheta)/\pi = (0.5, 0)$ . Here, the bar over  $\mathcal{F}$  means averaging over repeated real-time detection and  $\langle \dots \rangle$  means averaging over all initial  $|X\rangle$  on the Bloch sphere. We consider realistic parameters  $\phi = 1.18\pi$  and  $\epsilon_D = 4\Delta$ , resulting in  $\hbar\omega(\phi) \simeq 0.89\Delta$ ,  $\varphi_0(\phi) \simeq 0.82\pi$ ,  $|\langle C_{0,1}(\phi) \rangle| \simeq 0.31$ ,  $I_{|0\rangle}/I_0 = -0.091$ , and  $I_{|1\rangle}/I_0 = 0.147$ . Other parameters are the same as Fig. 2.

which maximally fits  $I_{|X'\rangle} = I_{|X'\rangle}^S + A \sin \theta' \cos[\omega(\phi)(t - t_R) - \varphi_0(\phi) - \vartheta']$ . Despite the presence of a significant variance in time  $[\omega(\phi)\sigma_t = \pi/15]$  and supercurrent ( $\sigma_I/I_0 = 0.04$ ), which results in a relatively poor signal as depicted in the inset of Fig. 3(b), we still obtain small infidelity of approximately  $\bar{\mathcal{F}}(X, \sigma_t, \sigma_I) \sim 10^{-3}$  for fixed  $(\theta, \vartheta)/\pi = (0.5, 0)$ , where bar mark denotes averaging over repeated real-time detection of supercurrent, i.e.,  $\bar{\mathcal{F}}(X, \sigma_t, \sigma_I) \equiv \frac{1}{N_I} \sum_l \mathcal{F}(X, X_l')$  and  $|X_l'\rangle$  is the measured state of the  $l^{\text{th}}$  run detection with real-time supercurrent  $I_{|X\rangle}^l(t_n)$ . The infidelity can be reduced when  $\theta$  approach 0 and  $\pi$ , reaching  $\bar{\mathcal{F}}(X, \sigma_t, \sigma_I) \sim 10^{-4}$ . Notably, the infidelity can be substantially reduced by increasing the total detection time  $t_D$  and by reducing the standard deviations in time and supercurrent, as shown in Fig. 3(b), where  $\langle \bar{\mathcal{F}}(\sigma_t, \sigma_I) \rangle \equiv \frac{1}{N_X} \sum_X \bar{\mathcal{F}}(X, \sigma_t, \sigma_I)$  means averaging over all  $|X\rangle$  on the Bloch sphere. We have double checked that the order of the averages taken commute,

i.e., first over the runs then over the Bloch sphere. The preparation infidelity of the qubit states is order of  $10^{-3}$ , enough for large-scale quantum computing, which can be effectively detected by our readout techniques. Consequently, our proposed non-collapsing readout scheme for the Andreev qubit is experimentally achievable and remains robust against the experimental errors.

## VI. CONCLUSION

We proposed a protocol to sense non-destructively an arbitrary state of an Andreev qubit. Our proposal does not use ancilla qubits, ubiquitous in nondemolition measurement protocols. Quite remarkably, our readout does not collapse the Andreev qubit state and hence avoids erasing its stored quantum information upon sensing it. Through a detailed calculation, we have shown that our detection protocol relies entirely on the sizable ordinary electrical supercurrent arising from the superposition encoded in the Andreev qubit. This supercurrent consists of static and dynamic contributions. The latter arises from the interference between the quantum many-body states defining the Andreev qubit superposition; it is oscillatory like the AC Josephson supercurrent and can be even larger than the static component. Because the detection of the Andreev qubit state is not only non-destructive but also non-collapsing, our proposed qubit sensing has a huge advantage over nondemolition protocols. More specifically, our readout protocol does away with the ancilla qubit overhead (preparation, information transfer, measurements, etc). More importantly, it enables one to obtain – for each run with a distinct singly prepared initial qubit state on the Bloch sphere – all subsequent readouts of the qubit state in the time window of interest. This reduces dramatically the overhead of repetitive qubit resetting in standard approaches that collapse the qubit state. Finally, by simulating experimental non-idealities, we showed that our readout protocol has fidelities within the usual quantum error-correction thresholds. We believe our proposal greatly streamlines the readout process and potentially improves the overall efficiency in quantum information processing tasks using Andreev qubits, thus promoting them as a viable platform.

## ACKNOWLEDGEMENT

This work is supported by National Key R&D Program of China (Grant Nos. 2020YFA0308800, 2021YFA1401500), the Hong Kong Research Grants Council (Grant Nos. 16306220, 16304523), the National Natural Science Foundation of China (Grant Nos. 12234003, 12321004, 12022416, 12475015, 11875108), the National Council for Scientific and Technological Development (Grant No. 301595/2022-4) and the São Paulo Research Foundation (Grant No. 2020/00841-9).

- 
- [1] A. Zazunov, V. Shumeiko, E. Bratus, J. Lantz, and G. Wendin, Andreev level qubit, *Phys. Rev. Lett.* **90**, 087003 (2003).
- [2] N. M. Chtchelkatchev and Y. V. Nazarov, Andreev quantum dots for spin manipulation, *Phys. Rev. Lett.* **90**, 226806 (2003).
- [3] L. Bretheau, Ç. Girit, H. Pothier, D. Esteve, and C. Urbina, Exciting andreev pairs in a superconducting atomic contact, *Nature* **499**, 312 (2013).
- [4] D. Willsch, D. Rieger, P. Winkel, M. Willsch, C. Dickel, J. Krause, Y. Ando, R. Lescanne, Z. Leghtas, N. T. Bronn, *et al.*, Observation of josephson harmonics in tunnel junctions, *Nat. Phys.* , 1 (2024).
- [5] M. Pita-Vidal, A. Bargerbos, R. Zitko, L. J. Splitthoff, L. Grünhaupt, J. J. Wesdorp, Y. Liu, L. P. Kouwenhoven, R. Aguado, B. van Heck, *et al.*, Direct manipulation of a superconducting spin qubit strongly coupled to a transmon qubit, *Nat. Phys.* **19**, 1110 (2023).
- [6] A. Bernard, Y. Peng, A. Kasumov, R. Deblock, M. Ferrier, F. Fortuna, V. Volkov, Y. A. Kasumov, Y. Oreg, F. von Oppen, *et al.*, Long-lived andreev states as evidence for protected hinge modes in a bismuth nanoring josephson junction, *Nat. Phys.* **19**, 358 (2023).
- [7] L. Bretheau, Ç. Girit, C. Urbina, D. Esteve, and H. Pothier, Supercurrent spectroscopy of andreev states, *Phys. Rev. X* **3**, 041034 (2013).
- [8] X.-P. Zhang, Renormalized and iterative formalism of the andreev levels within large multiparametric space, arXiv preprint arXiv:2405.02908 <https://doi.org/10.48550/arXiv.2405.02908> (2024).
- [9] C. Janvier, L. Tosi, L. Bretheau, Ç. Girit, M. Stern, P. Bertet, P. Joyez, D. Vion, D. Esteve, M. Goffman, *et al.*, Coherent manipulation of andreev states in superconducting atomic contacts, *Science* **349**, 1199 (2015).
- [10] L. Tosi, C. Metzger, M. Goffman, C. Urbina, H. Pothier, S. Park, A. L. Yeyati, J. Nygård, and P. Krogstrup, Spin-orbit splitting of andreev states revealed by microwave spectroscopy, *Phys. Rev. X* **9**, 011010 (2019).
- [11] M. Hays, V. Fatemi, D. Bouman, J. Cerrillo, S. Diamond, K. Serniak, T. Connolly, P. Krogstrup, J. Nygård, A. L. Yeyati, A. Geresdi, and M. H. Devoret, Coherent manipulation of an andreev spin qubit, *Science* **373**, 430 (2021).
- [12] G. Wendin and V. Shumeiko, Coherent manipulation of a spin qubit, *Science* **373**, 390 (2021).
- [13] F. J. Matute-Cañadas, C. Metzger, S. Park, L. Tosi, P. Krogstrup, J. Nygård, M. F. Goffman, C. Urbina, H. Pothier, and A. L. Yeyati, Signatures of interactions in the andreev spectrum of nanowire josephson junctions, *Phys. Rev. Lett.* **128**, 197702 (2022).
- [14] M. Hays, V. Fatemi, K. Serniak, D. Bouman, S. Diamond, G. de Lange, P. Krogstrup, J. Nygård, A. Geresdi, and M. Devoret, Continuous monitoring of a trapped superconducting spin, *Nat. Phys.* **16**, 1103 (2020).
- [15] C. Metzger, S. Park, L. Tosi, C. Janvier, A. A. Reynoso, M. Goffman, C. Urbina, A. L. Yeyati, and H. Pothier, Circuit-qed with phase-biased josephson weak links, *Phys. Rev. Res.* **3**, 013036 (2021).
- [16] M. A. Nielsen and I. L. Chuang, *Quantum computation and quantum information* (Cambridge university press, 2010).
- [17] W. K. Wootters and W. H. Zurek, A single quantum cannot be cloned, *Nature* **299**, 802 (1982).
- [18] V. B. Braginsky, Y. I. Vorontsov, and K. S. Thorne, Quantum nondemolition measurements, *Science* **209**, 547 (1980).
- [19] V. B. Braginsky and F. Y. Khalili, Quantum nondemolition measurements: the route from toys to tools, *Rev. Mod. Phys.* **68**, 1 (1996).
- [20] X. Xue, B. D’Anjou, T. F. Watson, D. R. Ward, D. E. Savage, M. G. Lagally, M. Friesen, S. N. Coppersmith, M. A. Eriksson, W. A. Coish, and L. M. K. Vandersypen, Repetitive quantum nondemolition measurement and soft decoding of a silicon spin qubit, *Phys. Rev. X* **10**, 021006 (2020).
- [21] T. Meunier, I. T. Vink, L. H. Willems van Beveren, F. H. L. Koppens, H. P. Tranitz, W. Wegscheider, L. P. Kouwenhoven, and L. M. K. Vandersypen, Nondestructive measurement of electron spins in a quantum dot, *Phys. Rev. B* **74**, 195303 (2006).
- [22] T. Nakajima, A. Noiri, J. Yoneda, M. R. Delbecq, P. Stano, T. Otsuka, K. Takeda, S. Amaha, G. Allison, K. Kawasaki, *et al.*, Quantum non-demolition measurement of an electron spin qubit, *Nat. Nanotechnol.* **14**, 555 (2019).
- [23] D. J. Wineland, Nobel lecture: Superposition, entanglement, and raising schrödinger’s cat, *Rev. Mod. Phys.* **85**, 1103 (2013).
- [24] D. B. Hume, T. Rosenband, and D. J. Wineland, High-fidelity adaptive qubit detection through repetitive quantum nondemolition measurements, *Phys. Rev. Lett.* **99**, 120502 (2007).
- [25] S. Haroche, Nobel lecture: Controlling photons in a box and exploring the quantum to classical boundary, *Rev. Mod. Phys.* **85**, 1083 (2013).
- [26] G. Nogues, A. Rauschenbeutel, S. Osnaghi, M. Brune, J.-M. Raimond, and S. Haroche, Seeing a single photon without destroying it, *Nature* **400**, 239 (1999).
- [27] D. Niemietz, P. Farrera, S. Langenfeld, and G. Rempe, Nondestructive detection of photonic qubits, *Nature* **591**, 570 (2021).
- [28] A. L. Andersen and K. Mølmer, Quantum nondemolition measurements of moving target states, *Phys. Rev. Lett.* **129**, 120402 (2022).
- [29] L. Jiang, J. Hodges, J. Maze, P. Maurer, J. Taylor, D. Cory, P. Hemmer, R. L. Walsworth, A. Yacoby, A. S. Zibrov, *et al.*, Repetitive readout of a single electronic spin via quantum logic with nuclear spin ancillae, *Science* **326**, 267 (2009).
- [30] P. Neumann, J. Beck, M. Steiner, F. Rempp, H. Fedder, P. R. Hemmer, J. Wrachtrup, and F. Jelezko, Single-shot readout of a single nuclear spin, *science* **329**, 542 (2010).
- [31] L. Robledo, L. Childress, H. Bernien, B. Hensen, P. F. Alkemade, and R. Hanson, High-fidelity projective readout of a solid-state spin quantum register, *Nature* **477**, 574 (2011).
- [32] P. C. Maurer, G. Kucsko, C. Latta, L. Jiang, N. Y. Yao, S. D. Bennett, F. Pastawski, D. Hunger, N. Chisholm, M. Markham, *et al.*, Room-temperature quantum bit memory exceeding one second, *Science* **336**, 1283 (2012).
- [33] J. M. Boss, K. Cujia, J. Zopes, and C. L. Degen, Quantum sensing with arbitrary frequency resolution, *Science*

- 356, 837 (2017).**
- [34] A. Lupaşcu, S. Saito, T. Picot, P. De Groot, C. Harmans, and J. Mooij, Quantum non-demolition measurement of a superconducting two-level system, *Nat. Phys.* **3**, 119 (2007).
- [35] B. Johnson, M. Reed, A. A. Houck, D. Schuster, L. S. Bishop, E. Ginossar, J. Gambetta, L. DiCarlo, L. Frunzio, S. Girvin, *et al.*, Quantum non-demolition detection of single microwave photons in a circuit, *Nat. Phys.* **6**, 663 (2010).
- [36] S. S. Elder, C. S. Wang, P. Reinhold, C. T. Hann, K. S. Chou, B. J. Lester, S. Rosenblum, L. Frunzio, L. Jiang, and R. J. Schoelkopf, High-fidelity measurement of qubits encoded in multilevel superconducting circuits, *Phys. Rev. X* **10**, 011001 (2020).
- [37] O. Kürtössy, Z. Scherübl, G. Fülöp, I. E. Lukács, T. Kanne, J. Nygård, P. Makk, and S. Csonka, Andreev molecule in parallel InAs nanowires, *Nano Lett.* **21**, 7929 (2021).
- [38] S. Vaitiekėnas, Y. Liu, P. Krogstrup, and C. Marcus, Zero-bias peaks at zero magnetic field in ferromagnetic hybrid nanowires, *Nat. Phys.* **17**, 43 (2021).
- [39] X.-P. Zhang, Fabry-perot superconducting diode, *Phys. Rev. B* **109**, 184513 (2024).
- [40] X.-P. Zhang and Y. Yao, Fermi sea and sky in the bogoliubov-de gennes equation, *arXiv preprint arXiv:2404.07423* (2024).
- [41] M. H. Cohen, L. M. Falicov, and J. C. Phillips, Superconductive tunneling, *Phys. Rev. Lett.* **8**, 316 (1962).
- [42] V. Ambegaokar and A. Baratoff, Tunneling between superconductors, *Phys. Rev. Lett.* **10**, 486 (1963).
- [43] Supplementary information, for details of the derivations of dynamic interference supercurrent which includes Refs. [39, 41, 42, 51, 52].
- [44] P. F. Bagwell, Suppression of the josephson current through a narrow, mesoscopic, semiconductor channel by a single impurity, *Phys. Rev. B* **46**, 12573 (1992).
- [45] C. Beenakker, Universal limit of critical-current fluctuations in mesoscopic josephson junctions, *Phys. Rev. Lett.* **67**, 3836 (1991).
- [46] C. Beenakker, D. Pikulin, T. Hyart, H. Schomerus, and J. Dahlhaus, Fermion-parity anomaly of the critical supercurrent in the quantum spin-hall effect, *Phys. Rev. Lett.* **110**, 017003 (2013).
- [47] R. Grasset, K. Katsumi, P. Massat, H.-H. Wen, X.-H. Chen, Y. Gallais, and R. Shimano, Terahertz pulse-driven collective mode in the nematic superconducting state of  $\text{Ba}_1\text{-xkxFe}_2\text{As}_2$ , *npj Quantum Materials* **7**, 4 (2022).
- [48] Y. Yang, R. B. Wilson, J. Gorchon, C.-H. Lambert, S. Salahuddin, and J. Bokor, Ultrafast magnetization reversal by picosecond electrical pulses, *Science Advances* **3**, e1603117 (2017), <https://www.science.org/doi/pdf/10.1126/sciadv.1603117>.
- [49] R. Matsunaga, N. Tsuji, H. Fujita, A. Sugioka, K. Makise, Y. Uzawa, H. Terai, Z. Wang, H. Aoki, and R. Shimano, Light-induced collective pseudospin precession resonating with higgs mode in a superconductor, *Science* **345**, 1145 (2014), <https://www.science.org/doi/pdf/10.1126/science.1254697>.
- [50] X. Yang, C. Vaswani, C. Sundahl, M. Mootz, L. Luo, J. H. Kang, I. E. Perakis, C. B. Eom, and J. Wang, Lightwave-driven gapless superconductivity and forbidden quantum beats by terahertz symmetry breaking, *Nat. Photonics* **13**, 707 (2019).
- [51] W. Kirk, *Nanostructures and mesoscopic systems* (Academic Press, 2012).
- [52] M. C. Dartiailh, W. Mayer, J. Yuan, K. S. Wickramasinghe, A. Matos-Abiague, I. Žutić, and J. Shabani, Phase signature of topological transition in josephson junctions, *Phys. Rev. Lett.* **126**, 036802 (2021).